Solar Energy Materials & Solar Cells 132 (2015) 329–336

Contents lists available at ScienceDirect

Solar Energy Materials & Solar Cells

journal homepage: www.elsevier.com/locate/solmat

Gasochromic effect in colloidal nanoparticles of tungsten oxide dihydrate synthesized via a simple anodizing method

M. Ranjbar *, A. Heidari Fini, H. Kalhori, P. Kameli, H. Salamati

Department of Physics, Isfahan University of Technology, Isfahan 84156-83111, Iran

ARTICLE INFO

Article history:
Received 26 May 2014
Received in revised form
29 August 2014
Accepted 10 September 2014

Keywords:
Anodizing
Tungsten oxide dehydrate
Gasochromic
XRD
XPS
HRTEM

ABSTRACT

This paper reports the gasochromic effect in colloidal nanoparticles of tungsten oxide dihydrate synthesized via a simple electrochemical anodizing of tungsten in an electrolyte composed of 0.02 M HCl. The anodizing caused the electrolyte to convert to a light yellowish colloidal solution consisting of tungsten oxide dihydrate. The ultimate gasochromic colloidal solutions were obtained just by addition of different volumes of 0.2 g/l $PdCl_2$ solution as a source of hydrogen catalyst into the primary colloidal tungsten dihydrate solution. Different tools involving, X-ray diffraction (XRD), high-resolution transmission electron microscope (HRTEM), X-ray photoelectron spectroscopy (XPS), and furrier transformed infrared (FTIR) spectroscopy characterized the colloidal nanoparticles. XRD measurements revealed that the as-prepared nanoparticles are monoclinic $WO_3 \cdot 2(H_2O)$ and were converted to monoclinic WO_3 by annealing at temperatures above 300 °C. XPS showed that the hydroxyl groups and W^{5+} states are dominant in as-prepared sample and lower after annealing or loading $PdCl_2$. It was observed that the Pd-$WO_3 \cdot 2(H_2O)$ solutions which were colorless initially, turned into blue color after dilute hydrogen insertion and then into the colorless state by spontaneously bleaching in ambient air. Moreover, no coloring was observed for colloidal solution composed of monoclinic WO_3. The optical absorption spectra of colloidal samples in colored states were composed of three certain distinct absorption peaks located at 1.3, 1.6 and 1.9 eV. The intensities of first and third peaks were comparable and dominant at deep blue states but, upon bleaching, the second one gradually overcomes them. We attributed this dynamical behavior to the possible surface and bulk phenomena. Finally, the obtained optical absorption results were compared with the small polaron hopping model.

1. Introduction

Recently tungsten oxide nanostructures have attracted more interests from scientific and technological viewpoints because of their sensing and catalytic properties as well as their electrochromic [1] and gasochromic [2] potential applications. In the gasochromic effect tungsten oxide thin films activated with a thin Pd or Pt layer switch from an optical colorless state to a dark blue absorbing state when they are exposed to dilute H_2 gas. This process is often reversible, because the colored films turn reversibly into the colorless state when H_2 is replaced with O_2 [2]. In addition to this observation, it should be noted that almost all the existing reports are commonly related to this effect with thin-film-type gasochromic devices.

Gasochromically or electrochemically colored films of tungsten oxide often show an optical absorption in the near infrared (NIR), which is a desirable effect for heat absorption applications in the solar systems such as thermal filters and building windows (smart windows) [3]. Most of the literature reports that focus their attention on the optical properties of colored films, declare that the NIR absorption includes a broad asymmetric peak at 1–1.5 eV range and various attempts have been made to find a valid explanation for it via peak-deconvolution by two or three multi-peaks [4].

Recently, we have introduced for the first time a gasochromic liquid composed of colloidal tungsten oxide nanoparticles as a new gasochromic system which has unique NIR absorption bands consisting of three main distinct peaks located at around 1.3, 1.6 and 1.9 eV [5]. Based on this observation, colloidal-type tungsten oxide seems to be more capable of acting than thin-film-type to assist basic studies of the gasochromic and hydrogen intercalation phenomena. In that study, crystalline tungsten oxide nanoparticles of about 40 nm average size have been directly

* Corresponding author. Tel.: +98 3113912375; fax: +98 3113912376.
E-mail address: ranjbar@cc.iut.ac.ir (M. Ranjbar).

http://dx.doi.org/10.1016/j.solmat.2014.09.016
0927-0248/

synthesized by pulsed laser ablation (PLA) method inside DI water and were activated against hydrogen gas by addition of small quantity of palladium salt ($PdCl_2$). Although PLA is a clean technique due to direct interaction of light with matter, but there are some disadvantages with this method such as the broad size distribution of produced nanoparticles, need for expensive equipments, and laser light attenuation as the liquid being opaque due to formation and spreading of nanoparticles.

The scope of this study is to extend the subject of gasochromic liquids into simpler, chipper and more productive synthesis methods. Moreover, to push the criteria toward understanding of fundamentals of the gasochromic mechanism, it is noteworthy that hydrate forms of tungsten oxide can be good candidates owing to their property of high proton transportation. For example, tungsten oxide dihydrate ($WO_3 \cdot 2(H_2O)$) lies in the series of good proton conductors at low operating temperatures and high humidity conditions [6].

Until now, different methods have been used for the synthesis of tungsten oxide nanoparticles including sol–gel [7], thermal oxidation [8], laser ablation in liquid [9], and wire explosion [10]. On the other hand, it has been demonstrated that electrochemical anodizing of tungsten sheets (plates and films) in certain (corrosive) media leads to formation of tungsten oxide hydrate surfaces over the sheets with porous structures and high surface/volume ratio on nanometer size scale. Anodizing has been vastly used for the fabrication of porous WO_3 films through an electrochemical process [11]. In the anodizing process we often deal with a working electrode (anode), reference electrode (cathode) and an electrolyte [12]. Applying electric field between the anode and cathode leads to anode corrosion through an oxidation process. To the best of our knowledge, the most studied electrochemical anodization trials of tungsten have been used for fabrication of a porous WO_3 layer over the anode surface [13–15]. In this study, we focus not on the anode surface, but instead on the materials released into the electrolyte medium from corrosive oxidation of the anode. The obtained solutions containing colloidal nanoparticles were used as the base of gasochromic liquid. Noble metals like palladium and platinum are well-known hydrogen catalysts. To make the system sensitive to hydrogen gas $PdCl_2$ aqueous solutions, as a palladium precursor, of different concentration was added into the above colloidal solutions. These mixtures were found to have gasochromic switching capability and were investigated in the current study by XRD, TEM, XPS, FTIR and UV–vis spectrophotometry.

2. Experimental

Nanoparticles of tungsten oxide dihydrate were fabricated by anodizing tungsten rods in diluted HCl. For this purpose, two tungsten rods were put 1 cm parallel to each other into a 0.02 M HCl electrolyte. Then a 60 V DC bias voltage were applied to the two ends of rods for 5 min (Fig. 1). By applying voltage, the anode surface began to corrode and was released gradually into the electrolyte. A $PdCl_2$ solution was prepared by adding 0.02 g of $PdCl_2$ powder (99.99% purity) into a mixture of 99.9 cc DI water and 0.1 cc HCl. This composition was kept in ultrasonic bath until $PdCl_2$ was dissolved and a uniform yellowish solution of 0.2 g/l $PdCl_2$ was obtained after 3 h. Then, various amounts of this solution including 0, 0.2, 0.4, 0.6, 0.8 and 1 cc, were added to 10 cc of as prepared colloidal solution of tungsten dihydrate. These obtained samples were named as WT5, WP0.2, WP0.4, WP0.6, WP0.8, and WP1 (Table 1). In order to perform some characterizations, samples were prepared by drop-drying the nanoparticles from their colloidal solution onto silicon or glass substrates. The crystalline structures were analyzed by X-ray diffraction ($Cu_{k\alpha}$, $\lambda = 0.1544$ nm, model Philips XPERT). Chemical bonds of the samples were obtained by FTIR spectroscopy in the mid-infrared range (600–4000 cm^{-1}) using Bruker FTIR (model Tensor27) system. The XPS analysis was done in an ESCA/AES system. The system is equipped with a concentric hemispherical analyzer (CHA, Specs model EA10 plus) suitable for auger electron spectroscopy and XPS. For exciting the X-ray photoelectrons, an AlK_α line at 1486.6 eV was used. The energy scale was calibrated against the carbon binding energy (284.8 eV). Optical properties of liquids before and after hydrogen intercalation were measured in the 190–1100 nm wavelength range using Perkin Elmer spectrophotometer (Lambda 25). The gasochromic experiments were carried out by alternatively bubbling 10%H_2/Ar (flow = 60 l/h) or O_2 (flow = 30 l/h) gases through a tiny stainless steel pipe into a quartz cell containing the colloidal samples.

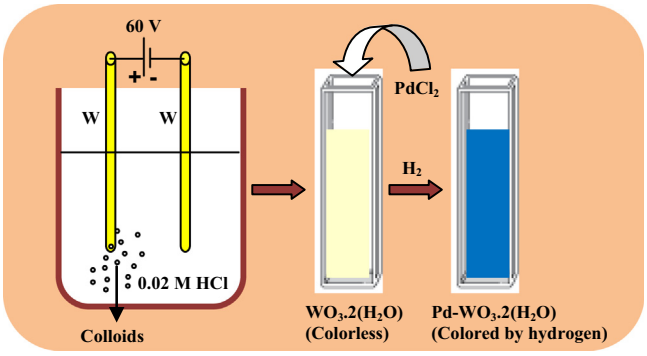

Fig. 1. Schematic representation of synthesis of $WO_3 \cdot 2(H_2O)$ colloidal solution by anodizing method, activation against hydrogen gas by $PdCl_2$ and gasochromic coloring by insertion of diluted hydrogen gas.

Table 1
Sample names and their preparation conditions.

Sample name		WT5	WP0.2	WP0.4	WP0.6	WP0.8	WP1
Anodizing time	(min)	5	5	5	5	5	5
$WO_3 \cdot 2(H_2O)$	(cc)	10	10	10	10	10	10
	(mmol/l)	2.5	2.5	2.5	2.5	2.5	2.5
$PdCl_2$ (0.2 g/l)	(cc)	0	0.2	0.4	0.6	0.8	1
	(μmol/l)	0	10	20	30	40	50

3. Result and discussion

3.1. Crystal structure

Fig. 2(a–g) shows the XRD patterns of as-prepared sample (WT5) before and after annealing at different temperatures of 100, 200, 300, 400 and 550 °C for 2 h in air. All the diffraction peaks of sample WT5 agree well with the monoclinic tungsten oxide dihydrate (PDF 00–016-0166), $WO_3 \cdot 2(H_2O)$. However, no intense diffraction peak has been detected after annealing at 100 °C. In addition, there are some weak peaks which could not be indexed, and are believed to be from the formation of an intermediate compounds during phase transition; likely orthorhombic tungsten oxide monohydrate with formula $WO_3 \cdot (H_2O)$. New diffraction peaks, however, appear in XRD pattern when annealing temperature increases to 200 °C. This pattern contains the diffraction peaks of the monoclinic WO_3 (PDF 00–005-0364) and indicates a significant crystalline transformation from the

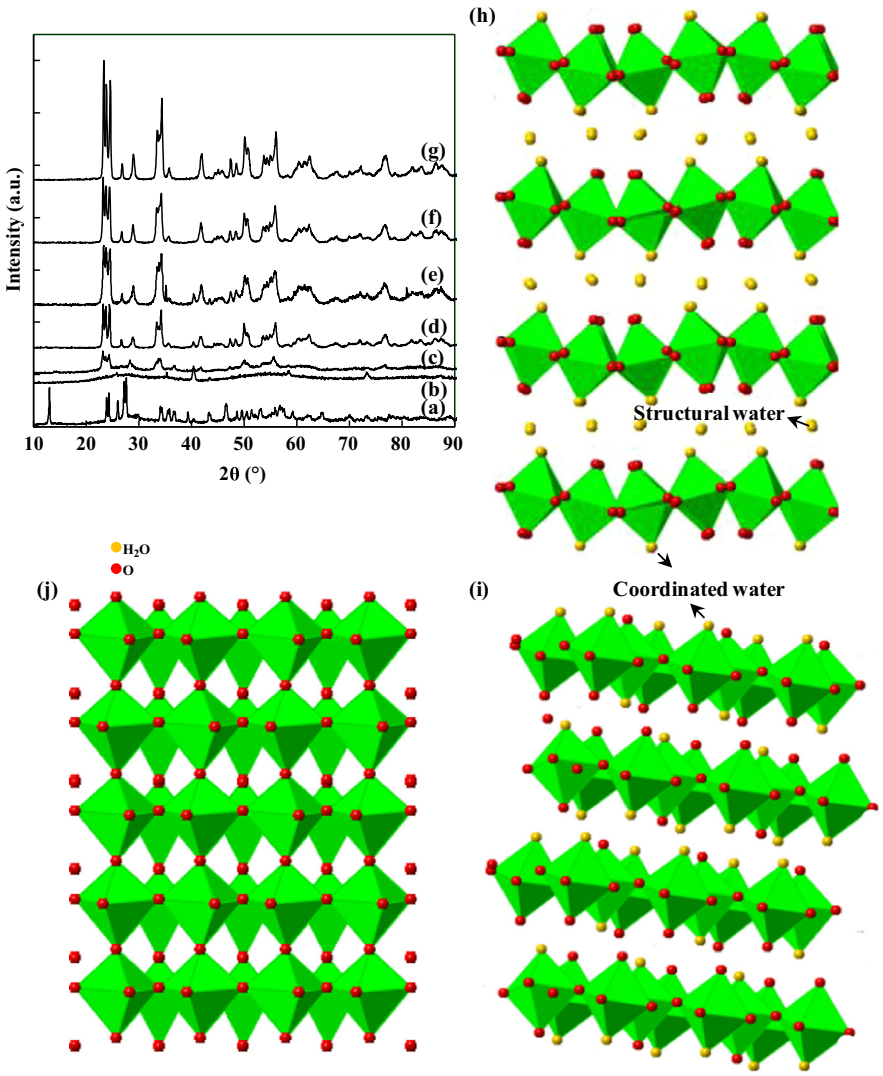

Fig. 2. XRD patterns of powder extracted from drop-drying of colloidal solution of tungsten oxide dihydrate (WT5) before (a) and after annealing at (b) 100, (c) 200, (d) 300, (e) 400, (f) 500 and (g) 550 °C. Crystal structure transform from monoclinic $WO_3 \cdot 2(H_2O)$ to monoclinic WO_3 upon annealing. Schematic representations of $WO_3 \cdot 2(H_2O)$ (h), $WO_3 \cdot (H_2O)$ (i) and monoclinic WO_3 (j).

dihydrate into the pure oxide phase at 200 °C. By increasing the annealing temperature to 300 °C, the diffraction peaks become sharper and narrower likely due to increase in crystallinity. The increased crystallinity also results in an increased density. Indeed, after annealing at temperatures above 300 °C monoclinic $WO_3 \cdot 2(H_2O)$ powder is completely converted to monoclinic WO_3 final phase. The schematic representations of the crystal structures of $WO_3 \cdot 2(H_2O)$, $WO_3 \cdot (H_2O)$ (which is the probable intermediate phase), and monoclinic WO_3 are shown in Fig. 2(h–j). From the graphical representations, each tungsten atom is surrounded by five oxygen atoms in both types of tungsten oxide hydrates and by six oxygen atoms in latter form of WO_3. The interpretations about oxygen bonding with tungsten or with water molecule will be used again when FTIR and XPS results are provided.

3.2. TEM

Fig. 3(a) shows a TEM image of sample WT5 and Fig. 3(b and c) shows two TEM images of sample WP0.6 with different magnifications. Parts (d) and (e) are size distribution histograms based on TEM images presented in parts (a) and (b). Sample WT5 has discrete nanoparticles while nanoparticles in sample WP0.6 were spontaneously assembled into chain-like arrangements. Moreover, in the high magnification image (part (c)), the dark spots can be attributed to the presence of metallic palladium NPs. It should be noted that very few separate particles have been found in TEM image series of this sample. Strong dipole–dipole interaction is believed to be the driving force of nanoparticle self-assembly and can be observed for noble metal nanoparticles surrounded by a negative double layer of charge [16]. Regarding the size distribution histograms (Fig. 3(d and e)) sample WT5 has a wide size distribution with 5.1 nm average size and sample WP0.6 has a narrower distribution with 4.8 nm average size. These findings show that Pd-WO_3 nanoparticles prefer to linearly aggregate with neighboring particles rather than to stay alone probably due to the presence of the palladium metallic phase.

HRTEM images of samples WT5 and WP0.6 are shown in Fig. 3 (g and h), respectively. Corresponding IFFT images obtained from some selected regions along with the *d*-spacing values are also shown at the insets of images. *d*-Spacing value of 2.4 was

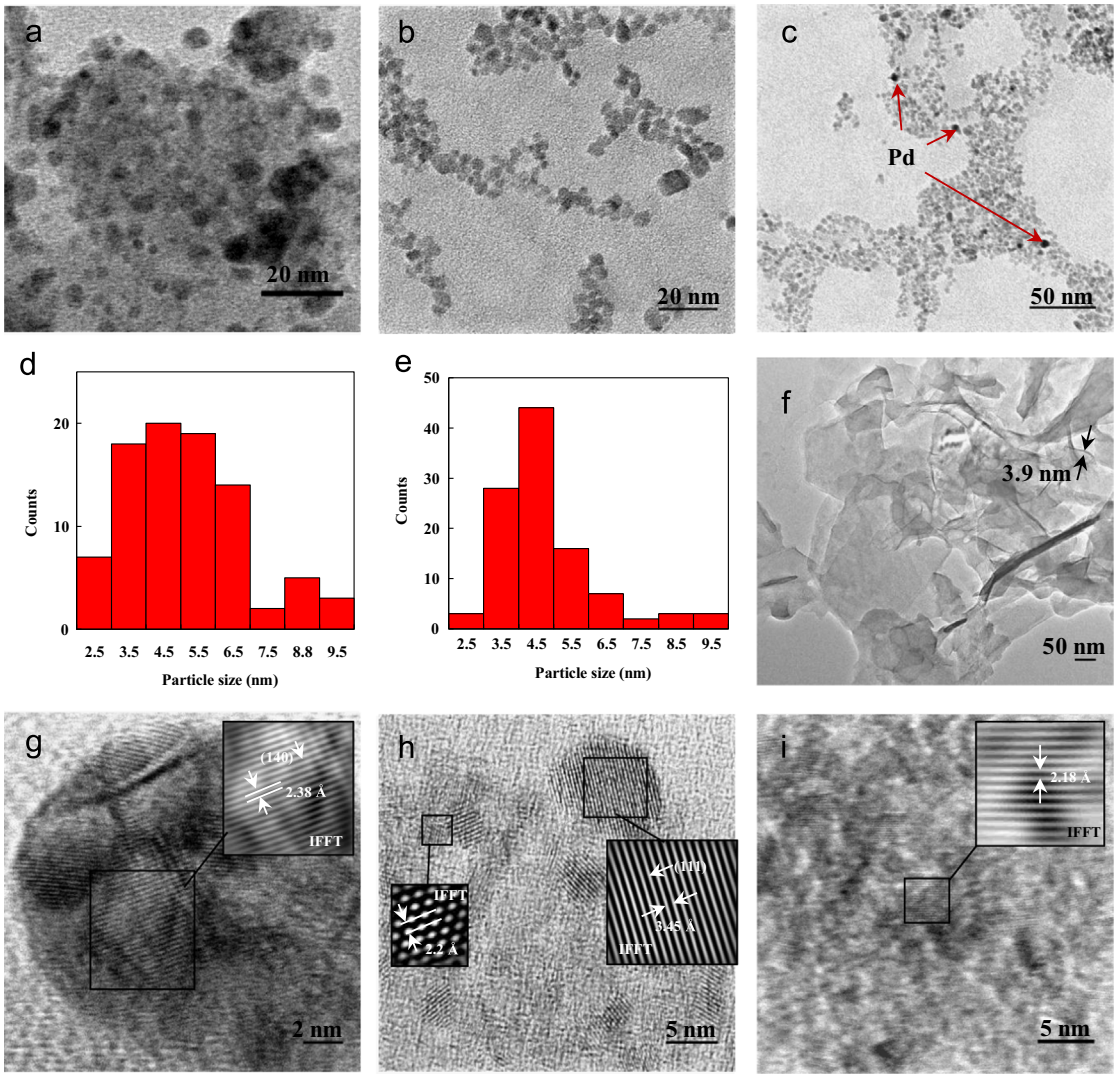

Fig. 3. TEM images of (a) sample WT5, (b and c) two TEM images of sample WP0.6 with different magnifications, (d) and (e) size distribution histograms of samples corresponding to parts (a) and (b), respectively, (f) TEM images of the WT5 after annealing at 550 °C. HRTEM images of sample WT5 (g), sample WP0.6 (h) and sample WT5 after annealing at 550 °C.

estimated in part (g) which is assigned to (140) crystallographic ordination of tungsten oxide dihydrate. The value of 3.4 Å in part (h) is attributed to the (111) orientation. Moreover, IFFT image processed for a particle of dark spots has *d*-spacing of about 2.2 Å which is related to Pd (111) crystallographic orientations.

TEM images of the WT5 after annealing at 550 °C (part (f)) consists of plate-like nanostructures. The sheets thickness can be approximated from the edges of some curved plates, which is about 3.9 nm shown by arrows. The corresponding HRTEM image is shown in Fig. 3(i). As can be seen from IFFT, the obtained *d*-spacing value is about 2.2 Å which is assigned to (−222) orientation of monoclinic WO_3.

3.3. FTIR

Fig. 4 shows the FTIR spectra of the sample WT5 before and after annealing at 550 °C, and the sample WP0.6 before and after one coloring–bleaching cycle. The FTIR spectra of before annealing (parts (a–c)) are almost similar and show different peaks located at around 656, 911, 985, and 1623 cm^{-1}. According to the literature, the first vibration band is related to corner sharing ν(W–O–W) mode [17] and the second and third ones to the vibration of ν(O–W–O) stretching mode and terminal ν(W═O), respectively [17,18]. The peak positions and relative intensities remain almost unchanged after addition of palladium salt or after hydrogen insertion–extraction process in the single gasochromic cycle. It has been shown elsewhere for tungsten oxide films that the crystal structure of colored and bleached states are often different [19]. This part of FTIR results demonstrates that probably the chemical and structural transitions are reversible processes in the gasochromic effect. However, these three vibrations undergo slight shifts toward lower wavenumbers of 642, 817 and 923 cm^{-1} after annealing. Moreover, the relative intensities of these three peaks vary in the process of annealing (part (d)) due to change in chemical bonds.

The vibration band at 1623 cm^{-1} is related to (W–OH) hydroxyl groups that diminishes, as shown in part (d), after annealing process. Moreover, there are two stretching modes in the range of 3100–3500 cm^{-1}. This frequency range is related to vibration modes of H_2O molecules [20]. Indeed, the structure of tungsten oxide dihydrate displays two kinds of water molecules (see Fig. 2 (h)); coordinated water and structural water. The coordinated H_2O

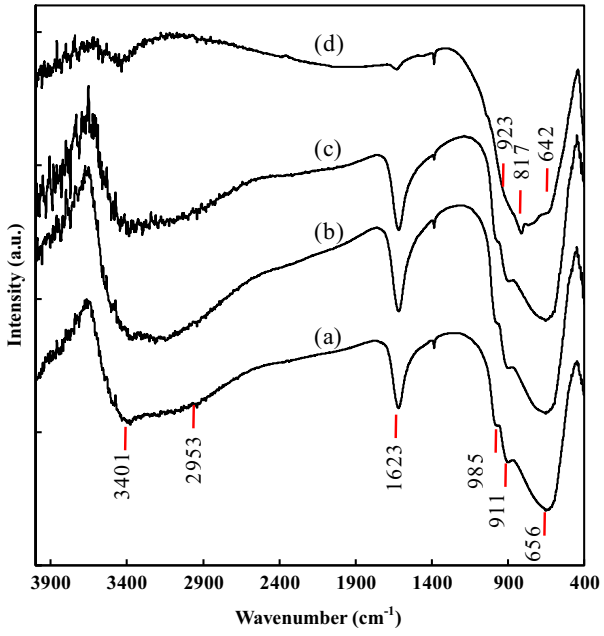

Fig. 4. FTIR spectra of the sample WT5 before (a) and after annealing at 550 °C (b), and sample WP0.6 before (c) and after one coloring–bleaching cycle (d).

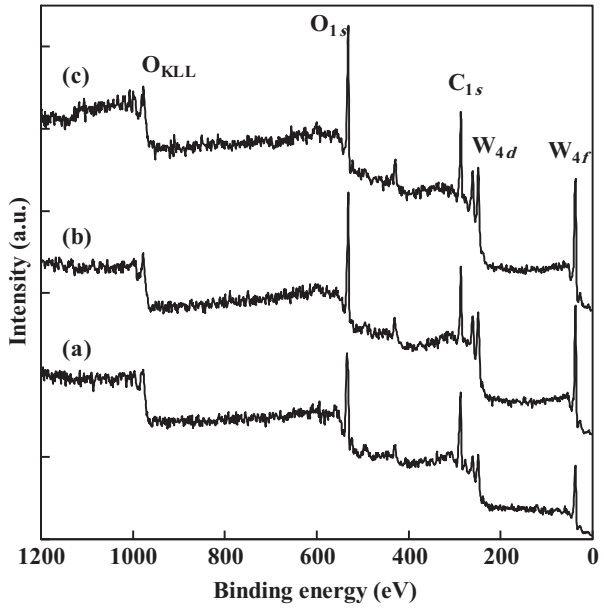

Fig. 5. XPS survey scan spectra of (a) sample WT5, (b) sample WP0.6 and (d) sample WT5 after annealing at 550 °C.

molecule is bonded to the lattice in coordinating octahedron round the tungsten ion, thus forming the $WO_5(OH_2)$ octahedron. Besides, those molecules that are arranged into an interlayer of water are called structural water. Each octahedron contains one terminal oxygen atom (W═O), one coordinating water molecule, and four bridging oxygen atoms connecting to the octahedra. The coordinated water frequency, in the case of $WO_3 \cdot 2(H_2O)$, is greater than that of structural water. Therefore, 2953 cm^{-1} vibrational frequency comes from coordinated water, and the other located at 3401 cm^{-1} is due to the structural water. As can be seen in Fig. 4(c), the structural water slightly weakens upon hydrogen

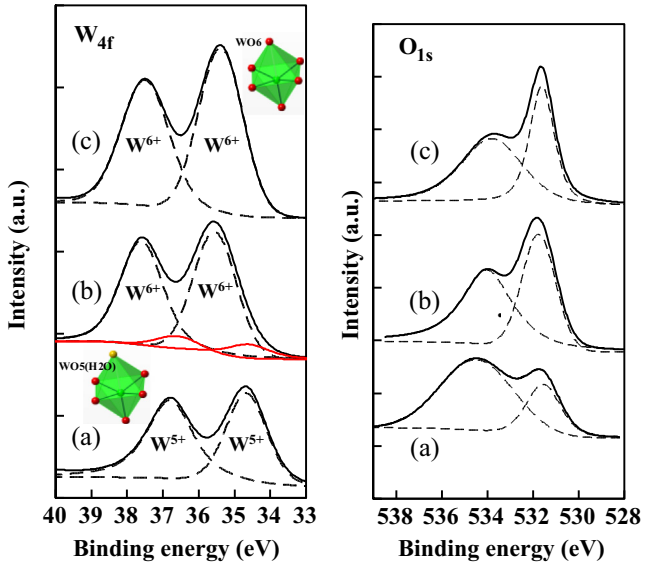

Fig. 6. High-resolution XPS spectra of W_{4f} and O_{1s} core levels. (a) sample WT5, (b) sample WP0.6, and (c) sample WT5 after annealing at 550 °C.

exposure. Probably the structural H_2O sites are preferential locations for hydrogen atoms to be absorbed.

3.4. XPS

The XPS survey scan spectra of samples WT5, taken before and after annealing at 550 °C, and WP0.6 are shown in Fig. 5(a–c). As can be seen, XPS signals of the elements W (35.7–37.7 eV), C (284.8 eV), and O (530–532 eV) exist in all the spectra. No signals of Pd or Cl were detected in palladium salt-containing sample within the detection limit of XPS, probably due to their low concentrations. The high-resolution XPS scans are able to analyze in detail the chemical states of each element. Corresponding high-resolution W_{4f} and O_{1s} XPS spectra are shown in Fig. 6(a–c). W_{4f} peaks can be deconvoluted into two or four (just for palladium salt-loaded sample, WP0.6) components depending on FWHMs of original peaks. These components are separated spin–orbit peaks of $W_{4f7/2}$ located at lower and $W_{4f5/2}$ at higher binding energies. The as-prepared sample (WT5) that was identified, according to XRD analysis, to be $WO_3 \cdot 2(H_2O)$ shows a doublet centered at 34.7 and 36.8 eV while for sample annealed at 550 °C they are shifted by 0.5 eV toward 35.6 and 37.7 eV higher energies, respectively. For as-prepared sample, according to literature, this doublet is originated from the presence of W^{5+} states [21]. Meanwhile, a general agreement exists for the binding energies of W^{6+} at 35.6 ± 0.2 and 37.7 ± 0.2 eV [21]. Moreover, the presence of W^{5+} state in sample WT5 is in consistent with illustrated crystal structure in the inset of Fig. 6, where W atoms are bonded to five oxygen atoms in $WO_5 \cdot (H_2O)$ octahedral and increases to six in WO_6 octahedral after annealing. The 0.5 eV shift toward the higher binding energies upon annealing is likely originated from chemical transformation of $WO_3 \cdot 2(H_2O)$ into WO_3 through desorption of coordinated water molecules.

In the case of sample WP0.6, there are four spin orbit peaks because the total FWHMs of its primary XPS spectra are wider than those of other two samples. The doublet with lower intensities is located at the same position as those of samples WT5 (W^{5+} states). However, the doublet of higher binding energies, i.e. W^{6+} states, has dominant peaks. The presence of W^{6+} states is attributed to the

oxidation of W^{5+} atoms in a reduction–oxidation reaction with palladium chloride. One can propose a half reaction for this conversion as below

$$Pd^{2+} + 2W^{5+} \rightarrow Pd^{0} + 2W^{6+} \quad (1)$$

In this half-reaction, palladium ions get electron from tungsten atoms and reduce to metallic palladium (see TEM images, Fig. 3) and at the same time, the oxidation number of tungsten increases from five to six.

The O_{1s} spectra acquired before annealing differ much more from after annealing. Before annealing, O_{1s} peak can be deconvoluted into two main peaks; one centered at 529.8 eV and one broad intense peak at 532.6 eV. The first one is related to oxygen bonding with tungsten atoms while the next one is due to the presence of O–H, O–C and/or oxygen contaminants absorbed the atmosphere [14]. After annealing, O_{1s} peak positions are 530.4 and 532.7 eV. In addition, the O–H peak intensity lowers considerably after annealing probably due to desorption of hydroxyl groups involving coordinated water. The O–H bonding remained even after annealing at 550 °C may originate from absorbed water and, according to XRD patterns which confirms phase transformation from $WO_3 \cdot 2(H_2O)$ to WO_3, cannot be due to structural water. This interpretation could be deduced from FTIR spectra (Fig. 4) too. Moreover, in O_{1s} XPS spectrum of sample WP0.6 the peak centered at 532 eV has lower relative intensity comparing with as-prepared sample WT5. Therefore, it seems that water molecules could be desorbed from the structure in the process of the oxidation–reduction reaction.

3.5. Gasochromic properties

Fig. 7(a and b) shows photographs of a typical sample in which the colorless solution turns blue after gasochromic coloring by 10 min hydrogen-containing gas exposure. To investigate the optical properties of gasochromically colored colloidal solutions prepared with different $PdCl_2$ concentrations, their optical absorption spectra were acquired and analyzed. Firstly, colorless samples were exposed to hydrogen gas for about 10 min, and then after the color saturated states were achieved, they were allowed to bleach spontaneously in air and the optical absorption spectra were recorded at different steps. The optical absorption spectra of blue states show some intense absorption peaks centered at photon energies of 1.3, 1.6, 1.9 eV and a weak shoulder at 2.4 eV (Fig. 8). For more clarity, we call these peaks as P_1, P_2, P_3 and P_4, respectively. Moreover, for the higher energy region above 3 eV, the absorption coefficient spectra of all the samples exhibit a sudden increase as the photon energy exceeds the band gap. The absorption spectra and time variation curves of peaks intensities are shown in Figs. 8(a–e) and 9(a–d), respectively for samples WP0.2, WP0.4, WP0.6, WP0.8 and WP1 at different bleaching steps. For sample WP0.2 at blue state, there is only a shoulder at 1.6 eV and a very weak peak at 1.3 eV with no considerable change in absorption spectra upon bleaching. Sample WP0.4 has three distinct absorption peaks at 1.3 (P_1), 1.6 (P_2) and 1.9 eV (P_3). In this case, the relative intensity of P_2 is low at the initial times of bleaching. However, the overall optical absorption reduces gradually and at the same time, the three distinct peaks change in intensity. The intensity variation of peaks is not uniform so that the diminish rate of P_1 and P_3 are faster than that of P_2. After about 7 min, the intensity of peak P_2 overcomes those of P_1 and P_3. Near the complete bleaching, after about 12 min, only one weak P_2 peak remains within the absorption spectrum. Now let's examine the situation in which palladium salt increases to higher concentrations. By increasing $PdCl_2$ volume to 0.6 cc (sample WP0.6) two absorption peaks P_1 and P_3 are only observable initially in which, comparing with sample WP0.4, P_2 has much low relative intensity. Corresponding time variation curves indicates that P_1 falling rate is faster than those of P_2 and P_3 (Fig. 9(b)). The intensity of P_2 is nearly constant for the first 8 min bleaching time but after about 12 min, it becomes the dominant peak.

In the cases of samples WP0.8 and WP1, as to the previous case, the peaks P_1 and P_3 are very strong at initial times but, upon bleaching, P_2 appears and becomes dominant. According to these findings, it is expected that a relation exists between hydrogen intercalation level and the shape and intensity of absorption peaks. Assuming proton formation rate depends on the Pd content in gasochromic effect, the hydrogen intercalation level not only is high at the initial colored stages, but also increases with the palladium salt concentration. Therefore, the presence of strong P_1–P_3 pairs and dominating P_2 can be related to hydrogen concentration variation from high to low quantities. Moreover, as one the most interesting consequences, the peak positions are constant during coloring–bleaching process for different sample types. The same peak positions were observed in our previous work on gasochromic colloidal solution prepared by laser ablation in water [5]. Therefore, the triplet peak of P_1–P_2–P_3 can be considered as an optical fingerprint for gasochromic colored colloidal tungsten oxide nanoparticles.

It should be noted that annealed samples, which were determined to be monoclinic WO_3 when dispersed in water again, did not show any gasochromic response (the results are not shown here). This indicates that structural or coordinated water play important role in gasochromic effect of colloidal nanoparticles.

Up to now, there is no unique model to satisfactorily describe the optical absorption in gasochromic coloring effect when hydrogen atoms are inserted into tungsten oxide. The papers on gasochromic thin films in literature propose different models including three band absorption [4], small polaron transition [22,23], double injection mechanisms [24] and a new model of oxygen vacancies [1]. In colloidal nanoparticles, as the present study, however, the situation is somewhat more complicated because the optical absorption spectra are composed of three discrete peaks located at certain energy positions with different intensities depending on hydrogen insertion level. However, it seems that there is a contradiction between the unvarying peaks positions in this report and small polaron transition model. Indeed the small polaron theory describing the coloring effect

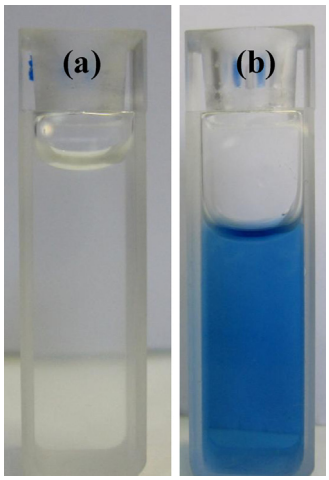

Fig. 7. Photograph of a typical colloidal solution of Pd-$WO_3 \cdot 2(H_2O)$ before (a) and after gasochromic coloring by 10 min hydrogen exposure (b).

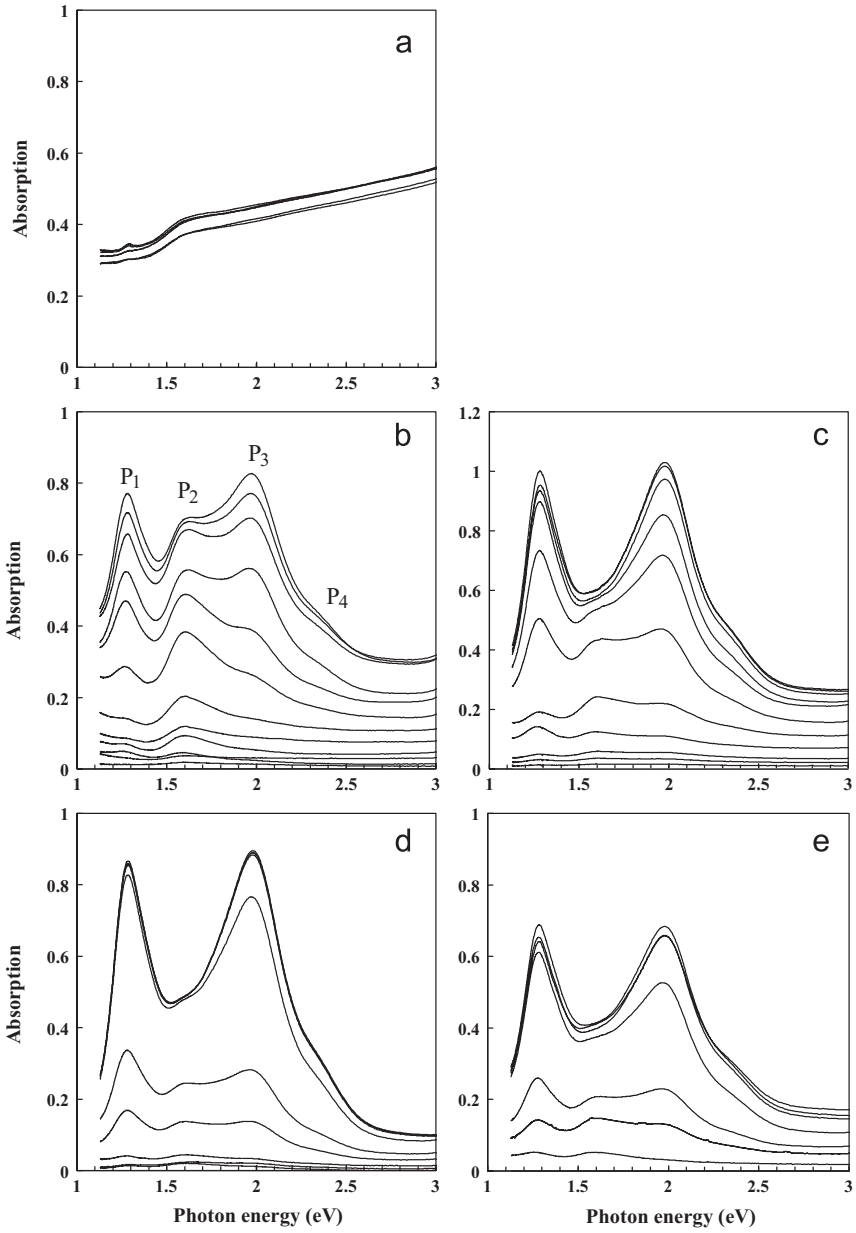

Fig. 8. Optical absorption spectra of samples (a) WP0.2, (b) WP0.4, (c) WP0.6, (d) WP0.8 and (e) WP1 at different steps of spontaneously bleaching in air.

in tungsten oxide films predicts that the polaron energies, hence the peak positions, vary with color center concentration which is proportional to the optical density. We believe that the three bands of absorption spectra are related to three pairs of possible tungsten oxide states including (W^{5+}, W^{4+}), (W^{5+}, W^{6+}) and (W^{4+}, W^{6+}). The intensity variation of the observed absorption peaks proposed that peak P_2, which is strong at low hydrogen insertion, is related to the surface phenomena while two other peaks are related to bulk phenomena. At full colored state, bulk effects are dominant firstly but upon bleaching, hydrogen atoms are gradually desorbed from the bulk and move toward the surface. As the hydrogen bulk concentration reduces to levels lower than that of surface, the surface effects become dominant. Nevertheless, to find an inclusive model for describing peaks positions and the dynamics of their variation the subject needs to be more studied both from experimental and theoretical points of view.

4. Conclusions

The results presented here illustrate the capability of anodizing method for synthesis of colloidal solution of tungsten oxide dihydrate nanoparticles with unique gasochromic properties. As a good hydrogen catalyst for gasochromic purposes, palladium was introduced into the colloidal solution by addition of aqueous $PdCl_2$. From HRTEM and XPS analyses, palladium salt is metalized spontaneously and increases the oxidation state of tungsten from W^{5+} to W^{6+} as well. An interesting gasochromic coloring developed within the colloidal Pd-containing tungsten dihydrate solution by bubbling of diluted hydrogen gas. The main aspects of the observed gasochromic effect are first the critical role of structural and/or coordinated water in arising gasochromic coloring and second the appearance of at least three distinct absorption bands in the near IR region. The peak positions were fixed during spontaneously bleaching in air but their relative intensities vary in different manners depending on

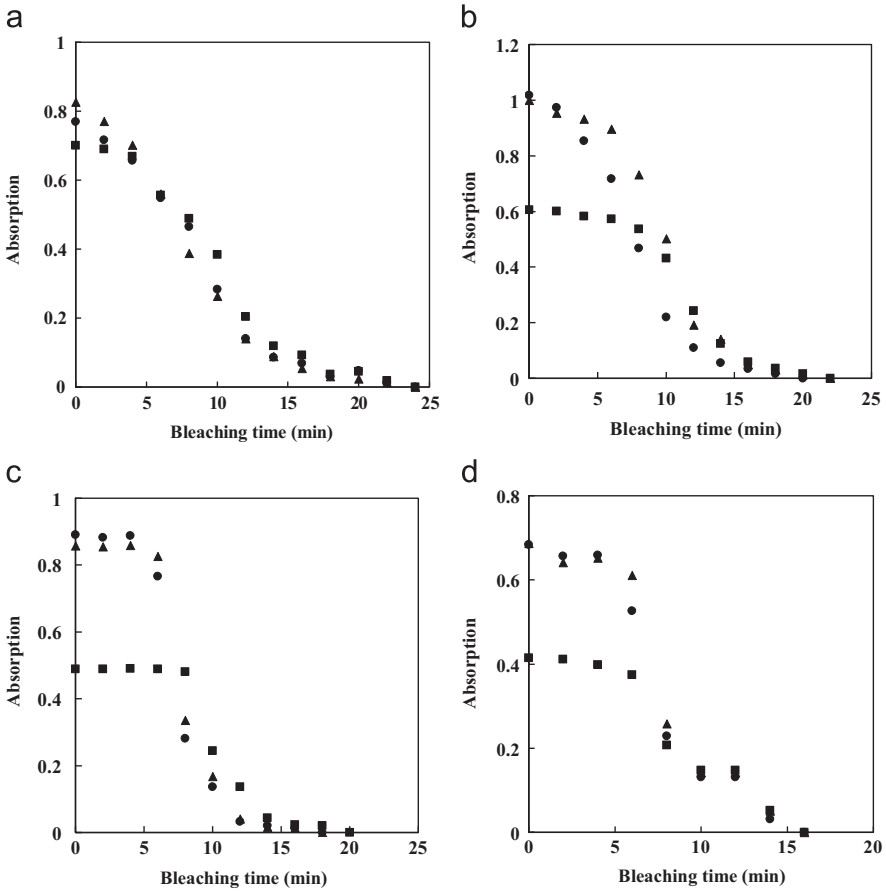

Fig. 9. Time variation curves of peaks intensities of samples colored states (a) WP0.4, (b) WP0.6, (c) WP0.8 and (d) WP1 upon spontaneously bleaching in air, P_1 (•), P_2 (■) and P_3 (▲).

hydrogen intercalation level. Although different models exist for describing gasochromic effect in tungsten oxide, but among them, data reported here is in contradiction with the small polaron theory.

Acknowledgment

The authors would like to thank the Iranian National Science Foundation (INSF) for their financial support.

References

[1] S.K. Deb, Opportunities and challenges in science and technology of WO_3 for electrochromic and related applications, Sol. Energy Mater. Sol. Cells 92 (2008) 245–258.
[2] A. Georg, W. Graf, V. Wittwer, Switchable windows with tungsten oxide, Vacuum 82 (2008) 730–735.
[3] V. Wittwer, M. Datz, J. Ell, A. Georg, W. Graf, G. Walze, Gasochromic windows, Sol. Energy Mater. Sol. Cells 84 (2004) 305–314.
[4] U. Tritthart, W. Gey, A. Gavrilyuk, Nature of the optical absorption band in amorphous $HxWO_3$ thin films, Electrochim. Acta 44 (1999) 3039–3049.
[5] M. Ranjbar, H. Kalhori, S.M. Mahdavi, A.I. Zad, New gasochromic system: nanoparticles in liquid, J. Nanopart. Res. 14 (2012) 803–902.
[6] Y.M. Li, M. Hibino, M. Miyayania, T. Kudo, Proton conductivity of tungsten trioxide hydrates at intermediate temperature, Solid State Ion. 134 (2000) 271–279.
[7] T. Kudo, H. Okamoto, K. Matsumoto, Y. Sasaki, Peroxopolytungstic acids synthesized by direct reaction of tungsten or tungsten carbide with hydrogen peroxide, Inorg. Chim. Acta 111 (1986) L27–L28.
[8] F. Galléa, Z. Li, Z. Zhang, Influence of deposition conditions on the morphology and phase of tungsten oxide nanorods synthesized by thermal oxidation, Front. Mater. Sci. China 1 (2007) 16–19.
[9] M. Ranjbar, H. Kalhori, S. Mahdavi, New gasochromic system: nanoparticles in liquid, J. Nanopart. Res. 14 (2012) 1–10.
[10] S. Aravinth, B. Sankar, S.R. Chakravarthi, R. Sarathi, Generation and characterization of nano tungsten oxide particles by wire explosion process, Mater. Charact. 62 (2011) 248–255.
[11] C.G. Granqvist, Handbook of Inorganic Electrochromic Materials, Elsevier, Amsterdam, 1995.
[12] J.O.M. Bockris, A.K. Reddy, Modern Electrochemistry: An Introduction to an Interdisciplinary Area, Springer, New York, 1973.
[13] A. Di Paola, F. Di Quarto, C. Sunseri, Electrochromism in anodically formed tungsten oxide films, J. Electrochem. Soc. 125 (1978) 1344–1347.
[14] J. Kukkola, J. Mäklin, N. Halonen, T. Kyllönen, G. Tóth, M. Szabó, A. Shchukarev, J.-P. Mikkola, H. Jantunen, K. Kordás, Gas sensors based on anodic tungsten oxide, Sens. Actuators B: Chem. 153 (2011) 293–300.
[15] K. Kalantar-zadeh, A. Vijayaraghavan, M.-H. Ham, H. Zheng, M. Breedon, M. S. Strano, Synthesis of atomically thin WO_3 sheets from hydrated tungsten trioxide, Chem. Mater. 22 (2010) 5660–5666.
[16] J. Liao, Y. Zhang, W. Yu, L. Xu, C. Ge, J. Liu, N. Gu, Linear aggregation of gold nanoparticles in ethanol, Colloids Surf. A: Physicochem. Eng. Asp. 223 (2003) 177–183.
[17] B. Orel, U.O. Krašovec, N. Grošelj, M. Kosec, G. Dražič, R. Reisfeld, Gasochromic behavior of sol–gel derived Pd doped peroxopolytungstic acid (W-PTA) nanocomposite films, J. Sol–gel Sci. Technol. 14 (1999) 291–308.
[18] C. Guery, C. Choquet, F. Dujeancourt, J. Tarascon, J. Lassegues, Infrared and X-ray studies of hydrogen intercalation in different tungsten trioxides and tungsten trioxide hydrates, J. Solid State Electrochem. 1 (1997) 199–207.
[19] H. Chen, N. Xu, S. Deng, D. Lu, Z. Li, J. Zhou, J. Chen, Gasochromic effect and relative mechanism of WO_3 nanowire films, Nanotechnology 18 (2007).
[20] Y. Li, M. Hibino, M. Miyayania, T. Kudo, Proton conductivity of tungsten trioxide hydrates at intermediate temperature, Solid State Ion. 134 (2000) 271–279.
[21] I. Martin-Litas, P. Vinatier, A. Levasseur, J.C. Dupin, Characterisation of r.f. sputtered tungsten disulfide and oxysulfide thin films, Thin Solid Films 416 (2002) 1–9.
[22] G.A. Niklasson, J. Klasson, E. Olsson, Polaron absorption in tungsten oxide nanoparticle aggregates, Electrochim. Acta 46 (2001) 1967–1971.
[23] O. Schirmer, V. Wittwer, G. Baur, G. Brandt, Dependence of WO_3 electrochromic absorption on crystallinity, J. Electrochem. Soc. 124 (1977) 749–753.
[24] S.-H. Lee, M.J. Seong, H.M. Cheong, E. Ozkan, E.C. Tracy, S.K. Deb, Effect of crystallinity on electrochromic mechanism of Li_xWO_3 thin films, Solid State Ion. 156 (2003) 447–452.